Available online at www.sciencedirect.com
SCIENCE DIRECT®
Journal of Solid State Chemistry 178 (2005) 3323–3335
JOURNAL OF SOLID STATE CHEMISTRY
www.elsevier.com/locate/jssc

$Ce_{10}[Si_{10}O_9N_{17}]Br$, $Nd_{10}[Si_{10}O_9N_{17}]Br$ and $Nd_{10}[Si_{10}O_9N_{17}]Cl$ oxonitridosilicate halides with a new layered structure type

Alexandra Lieb, Wolfgang Schnick*

Department Chemie und Biochemie, Lehrstuhl für Anorganische Festkörperchemie, Ludwig-Maximilians-Universität, Butenandtstraße 5–13 (D), D-81377 München, Germany

Received 3 June 2005; received in revised form 8 August 2005; accepted 17 August 2005
Available online 19 September 2005

Abstract

The isotypic oxonitridosilicate halides $Ce_{10}[Si_{10}O_9N_{17}]Br$, $Nd_{10}[Si_{10}O_9N_{17}]Br$ and $Nd_{10}[Si_{10}O_9N_{17}]Cl$ were obtained by the reaction of the respective lanthanide metals, their oxides and halides with "$Si(NH)_2$" in a radiofrequency furnace at temperatures around 1800 °C, using CsBr, resp. CsCl, as a flux. The crystal structures were determined by single-crystal X-ray diffraction (*Pbam*, no. 55, $Z = 2$; Ce/Br: $a = 10.6117(9)$ Å, $b = 11.2319(10)$ Å, $c = 11.688(8)$ Å, $R1 = 0.0356$; Nd/Br: $a = 10.523(2)$ Å, $b = 11.101(2)$ Å, $c = 11.546(2)$ Å, $R1 = 0.0239$; Nd/Cl: $a = 10.534(2)$ Å, $b = 11.109(2)$ Å, $c = 11.543(2)$ Å, $R1 = 0.0253$) and represent a new layered structure type. The structure refinements were performed utilizing an O/N-distribution model according to *Paulings* rules, i.e. nitrogen was positioned on all bridging sites and mixed O/N-occupation was assumed on the terminal sites resulting in charge neutrality of the compounds. The layers consist of condensed $[SiN_2(O/N)_2]$ and $[SiN_3(O/N)]$ tetrahedra of Q^2 and Q^3 type. The chemical composition of the compounds was derived from chemical analyses for $Nd_{10}[Si_{10}O_9N_{17}]Br$ and electron probe micro analyses (EPMA) for all three compounds. The results of IR spectroscopic investigations are reported.

Keywords: Cerium; Neodymium; Chloride; Bromide; Oxonitridosilicate; Crystal structure; Electron probe micro analysis (EPMA)

1. Introduction

Nitridosilicates derive from the classical oxosilicates by a formal exchange of oxygen by nitrogen. Typical building blocks of nitridosilicates are SiN_4 tetrahedra while oxosilicates are made up of SiO_4 units. Despite this analogy, there are more versatile structural variations concerning the interconnection of the tetrahedral building blocks in nitridosilicates [1,2]. Oxonitridosilicates (so-called "sions") represent an intermediate class of compounds between oxosilicates and nitridosilicates. They are of considerable interest for the development of inorganic materials for high performance applications owing to their structural diversity and their material properties (high thermal and chemical stability).

Chlorine containing oxosilicates are well known (e.g. the mineral Scapolite [3] and several other synthetic compounds [4–6]). Recently, we demonstrated that the incorporation of chloride in oxonitridosilicates is possible as well (i.e. $Ln_4[Si_4O_{3+x}N_{7-x}]Cl_{1-x}O_x$ (Ln = Ce, Pr, Nd) [7]). In the course of further systematical investigations, we recently discovered the first oxonitridosilicate bromides, i.e. $Ce_{10}[Si_{10}O_9N_{17}]Br$ and $Nd_{10}[Si_{10}O_9N_{17}]Br$. These compounds represent a new layered structure type and the first bromine-containing oxonitridosilicates so far. In addition we found that isotypic $Nd_{10}[Si_{10}O_9N_{17}]Cl$ also exists, which is an interesting example for anion substitution in that system.

2. Experimental

2.1. Syntheses

2.1.1. Synthesis of silicon diimide "$Si(NH)_2$"

Using "$Si(NH)_2$" instead of the relatively unreactive Si_3N_4 as starting material proved to be advantageous for

*Corresponding author. Fax: +49 89 2180 77440.
E-mail address: wolfgang.schnick@uni-muenchen.de (W. Schnick).

0022-4596/$ - see front matter © 2005 Elsevier Inc. All rights reserved.
doi:10.1016/j.jssc.2005.08.010

the synthesis of nitridosilicates and this also holds for sions and sialons [1,2,8]. "$Si(NH)_2$" was obtained by ammonolysis of $SiCl_4$ followed by a thermal treatment at 600 °C under an atmosphere of pure NH_3 (see Eq. (1) and (2)). A detailed description of the synthesis of "$Si(NH)_2$" is given in Ref. [8].

$$SiCl_4 + 6\,NH_3 \xrightarrow[NH_3\ \text{atmosphere}]{-78\,^\circ C} Si(NH)_2 + 4\,NH_4Cl, \quad (1)$$

$$Si(NH)_2 + 4NH_4Cl \xrightarrow[NH_3\ \text{atmosphere}]{600\,^\circ C,\ NH_4Cl} Si(NH)_2. \quad (2)$$

"$Si(NH)_2$" was obtained as an X-ray amorphous and reactive product. It is converted to amorphous Si_3N_4 at temperatures above 900 °C and thus it represents an important precursor compound for the technical production of Si_3N_4 ceramics [9].

2.1.2. Synthesis of $Ce_{10}[Si_{10}O_9N_{17}]Br$, $Nd_{10}[Si_{10}O_9N_{17}]Br$ and $Nd_{10}[Si_{10}O_9N_{17}]Cl$

$Ce_{10}[Si_{10}O_9N_{17}]Br$: A mixture of Ce (146 mg/1.0 mmol, Goodfellow, 99.99%, powder), "$Si(NH)_2$" (116 mg/2.0 mmol), $CeBr_3$ (298 mg/0.8 mmol, Chempur, 99.9%, ultradry), CeO_2 (154 mg/0.9 mmol, Chempur, 99.99%) and CsBr (1000 mg/4.7 mmol, Chempur, 99.99%) as a flux was thoroughly mixed and transferred into a tungsten crucible in a glove box (argon atmosphere). The crucible then was positioned in a water-cooled silica glass reactor of a radiofrequency furnace. It was heated under a pure nitrogen atmosphere to 1030 °C within 5 min, then to 1830 °C within 2 h, maintained at that temperature for 1 h and subsequently cooled to 1030 °C within 45 h. Finally, the product was quenched to room temperature.

The compounds $Nd_{10}[Si_{10}O_9N_{17}]Br$ and $Nd_{10}[Si_{10}O_9N_{17}]Cl$ were synthesized using analog mixtures: Nd/Br: Nd (108 mg/0.7 mmol, Chempur, 99.99%), "$Si(NH)_2$" (116 mg/2.0 mmol), $NdBr_3$ (300 mg/0.8 mmol, Chempur, 99.9%), Nd_2O_3 (200 mg/0.6 mmol, Chempur, 99.99%) and CsBr (1000 mg/4.7 mmol, Chempur, 99.99%); Nd/Cl: Nd (108 mg/0.7 mmol, Chempur, 99.99%), "$Si(NH)_2$" (116 mg/2.0 mmol), $NdCl_3$ (196 mg/0.8 mmol, Chempur, 99.9%), Nd_2O_3 (200 mg/0.6 mmol, Chempur, 99.99%) and CsCl (1000 mg/6 mmol, Chempur, 99.99%). The temperature treatment of the Nd/Br sample was similar to the Ce/Br sample. The Nd/Cl sample was heated to 1030 °C within 5 min, then to 1780 °C within 2 h, maintained at that temperature for 1 h and subsequently cooled to 1030 °C within 45 h. Finally, the product was quenched to room temperature. Further details about the experimental setup are given in Ref. [8].

The reactions yielded bundles of single crystals of needle-like shape (length up to 3 mm, diameter about 0.15 mm) together with small amounts of $Ln_3Si_6N_{11}$ [10–12], $Ln_2Si_3O_3N_4$ [13,14] and $Ln_4Si_2O_7N_2$ [15,16] as crystalline by-products. The crystals were of orange (Ce/Br) and pale violet (Nd/Br, Nd/Cl) colors, respectively. The compounds are completely stable against humidity and air.

2.2. Crystal-structure analysis

2.2.1. Single-crystal X-ray analysis

X-ray diffraction data of $Ce_{10}[Si_{10}O_9N_{17}]Br$, $Nd_{10}[Si_{10}O_9N_{17}]Br$ and $Nd_{10}[Si_{10}O_9N_{17}]Cl$ were collected using an IPDS diffractometer (STOE, Darmstadt) using Mo-K_α radiation. According to the observed reflection conditions ($0\,k\,l$ with $k = 2n$, $h\,0\,l$ with $h = 2n$, $h\,0\,0$ with $h = 2n$ and $0\,k\,0$ with $k = 2n$) of the orthorhombic lattice, the space group *Pbam* (no. 55) was determined. The second possible space group *Pba*2 (no. 32) has also been taken into account but led to a structure refinement that indicates a missing center of inversion. The structures were solved by direct methods using SHELXTL [17] and refined with anisotropic thermal displacement parameters for all atoms. The refinement of the light atoms (O, N) was performed according to *Paulings* rules [18] assuming N on all bridging positions (8*i*, 4*h*) and mixed O/N-occupancies of the terminal sites (8*i*, 4*g*), thus leading to charge neutrality of the compounds. Relevant crystallographic data and details of the X-ray data collection are shown in Table 1. Table 2 gives the positional and thermal displacement parameters for all atoms. Table 3 lists selected interatomic distances and angles.

Details of the single-crystal structure determinations of $Ce_{10}[Si_{10}O_9N_{17}]Br$, $Nd_{10}[Si_{10}O_9N_{17}]Br$ and $Nd_{10}[Si_{10}O_9N_{17}]Cl$ may be obtained from the Fachinformationszentrum Karlsruhe, D-76344 Eggenstein-Leopoldshafen, Germany, e-mail crysdata@FIZ-karlsruhe.de, by quoting the depository numbers CSD-415276, CSD-415275 and CSD-415274.

2.2.2. X-ray powder diffraction

Powder diffraction patterns were obtained from single-phase samples (ground single crystals) of $Ce_{10}[Si_{10}O_9N_{17}]Br$, $Nd_{10}[Si_{10}O_9N_{17}]Br$ and $Nd_{10}[Si_{10}O_9N_{17}]Cl$ using a STOE Stadi P diffractometer in Debye-Scherrer geometry utilizing glass capillaries (Hilgenberg, $\varnothing = 0.2$ mm). All of the detected reflections have been indexed and Rietveld refinements were performed using the GSAS program package [19]. A structural model based on the single-crystal structure data was employed. Relevant crystallographic data and details of the powder X-ray data collection are shown in Table 4. The refined powder patterns are shown in Fig. 1.

2.3. Chemical analysis and EPMA

The chemical analysis of $Nd_{10}[Si_{10}O_9N_{17}]Br$ was performed by Mikroanalytisches Labor Pascher, Remagen, Germany. Each element of the sample (30.2 mg) was analyzed twice, the results are listed in Table 5. Neodymium and silicon have been analyzed by means of ICP-AAS. For oxygen and nitrogen, the hot carrier gas extraction method was used. The bromine (resp. chlorine) content was determined by microtitration with Hg^{2+} solution.

Quantitative chemical analyses on the microscale by electron probe micro analysis (EPMA) were carried out

Table 1
Crystallographic data and details of the single crystal X-ray data collection for $Ce_{10}[Si_{10}O_9N_{17}]Br$, $Nd_{10}[Si_{10}O_9N_{17}]Br$ and $Nd_{10}[Si_{10}O_9N_{17}]Cl$

Lanthanide element, halide	Ce, Br	Nd, Br	Nd, Cl
Diffractometer, monochromator		STOE IPDS, graphite	
Radiation		MoK_α ($\lambda = 0.71073$ Å)	
Temperature/K		293(2)	
Space group		*Pbam*, orthorhombic	
Lattice parameters, a/Å	10.6117(9)	10.523(2)	10.534(2)
b/Å	11.2319(10)	11.101(2)	11.109(2)
c/Å	11.6288(8)	11.546(2)	11.543(2)
Cell volume, V/Å^3	1386.0(2)	1348.8(4)	1350.8(4)
Formula units		$Z = 2$	
Crystal size/mm^3	$0.299 \times 0.162 \times 0.159$	$0.144 \times 0.111 \times 0.075$	$0.113 \times 0.099 \times 0.067$
Crystal color	Orange	Pale violet	Pale violet
Calculated density/g cm^{-3}	5.138	5.381	5.264
Diffraction range/°	$5.28 < 2\theta < 60.82$	$5.34 < 2\theta < 60.62$	$5.32 < 2\theta < 60.54$
Measured reflections	13 935	13 676	13 468
Independent reflections	2176	2020	2103
Observed reflections	1919	1823	1839
Refined parameters	122	122	122
R_{int}	0.0531	0.0377	0.0344
$F(000)$	1892	1932	1896
Extinction coefficient, χ	0.0077(3)	0.0134(2)	0.00167(7)
Absorption correction		Semi-empirical, multiscan	
Absorption coefficient/mm^{-1}	17.975	20.866	19.457
Min./max. transmission	0.031/0.057	0.142/0.209	0.163/0.272
Min./max. residual electron density/e/Å^3	−2.786/3.689	−2.472/1.924	−2.654/2.905
GooF	1.017	1.098	1.030
R_1 [$I > 2\sigma(I)$]	0.0356 [0.0308]	0.0239 [0.0206]	0.0253 [0.0193]
wR_2 [$I > 2\sigma(I)$]	0.0802 [0.0782]	0.0520 [0.0512]	0.0448 [0.0437]

with the Jeol JXA-8900 R superprobe using an accelerating voltage of 15 kV, a beam current of 80 nA and a 3 μm measuring spot. The total volume analyzed was around 10–15 μm^3. The microprobe is equipped with synthetic multilayer spectrometer crystals with large d spacing for quantitative wavelength dispersive analysis of light elements. For N and O analysis, the LDE1 crystal with $2d = 600$ nm was used. Matrix correction was carried out with the CITZAF program [20]. For microprobe analysis, the samples were mounted with epoxy resin into cylindrical holes in an epoxy pellet of 25 mm diameter and polished with a final diamond powder grain size of 0.25 μm. The samples and the N standard were coated with carbon under high vacuum conditions simultaneously to ensure an identical carbon coat thickness for all of the samples. The carbon layer thickness of about 15 nm was controlled by interference colors on a polished brass surface.

Since the quantitative analysis of light elements such as N and O, and also of Cl and Br are not a routine EPMA technique (see [21,22]), significant care was taken to minimize errors that may occur during measurements of these low-energy X-ray emission lines. In addition, the analysis of light elements becomes more difficult in the presence of the various lanthanide elements in high concentrations in the analyzed oxonitridosilicates. The lanthanides produce a large number of emission lines which may overlap with the N, O or Cl $K\alpha$ lines. Further details of the measurements can be taken from Ref. [7]. The used standards are listed in Table 6.

2.4. Vibrational spectroscopy

FTIR spectra (Fig. 2) were measured at room temperature by using a Bruker IFS 66v/S spectrometer. The samples were thoroughly ground together with dried KBr (1 mg sample/250 mg KBr). The spectra unequivocally prove the absence of hydrogen (N–H).

3. Results and discussion

3.1. Chemical analysis and EPMA

The elemental analysis (Mikroanalytisches Labor Pascher, Remagen, Germany, proclaimed precision ≈0.3 weight% for O, N, Si, ≈0.2 weight% for Br, ≈1.0 weight% for Nd) for $Nd_{10}[Si_{10}O_9N_{17}]Br$ (Table 5) agrees well with the theoretical values for all elements.

Using EPMA, various crystals of $Ce_{10}[Si_{10}O_9N_{17}]Br$, $Nd_{10}[Si_{10}O_9N_{17}]Br$ and $Nd_{10}[Si_{10}O_9N_{17}]Cl$ were measured (≈30 spots on 5–7 grains). The averaged results are given in Table 7. The low values of 1 sigma indicate high homogeneity of the crystals. In addition, line scans were performed on needle-like crystals (10 spots per crystal), thus showing a homogeneous halide distribution of these

Table 2
Atomic coordinates and anisotropic displacement parameters (Å^2) for $Ce_{10}[Si_{10}O_9N_{17}]Br$, $Nd_{10}[Si_{10}O_9N_{17}]Br$ and $Nd_{10}[Si_{10}O_9N_{17}]Cl$ determined by single-crystal X-ray diffraction with e.s.d.s in parentheses

Atom	Wyck	x	y	z	s.o.f	U_{eq}	U_{11}	U_{22}	U_{33}	U_{23}	U_{13}	U_{12}
Ce1	8*i*	0.64253(3)	0.10224(3)	0.23527(3)	1	0.00659(11)	0.00529(16)	0.00556(16)	0.00891(17)	−0.00086(9)	−0.00049(9)	−0.00015(9)
Ce2	4*h*	0.87413(4)	0.12318(4)	0.5000	1	0.00832(12)	0.0093(2)	0.0087(2)	0.0070(2)	0	0	0.00332(14)
Ce3	4*e*	1	0	0.16742(3)	1	0.00665(12)	0.0077(2)	0.00661(19)	0.00560(19)	0	0	0.00115(14)
Ce4	4*g*	0.61555(4)	−0.12723(4)	0	1	0.00998(12)	0.0192(2)	0.00577(19)	0.0050(2)	0	0	0.00218(15)
Si1	8*i*	0.88471(13)	0.25734(12)	0.24655(11)	1	0.0048(3)	0.0043(6)	0.0056(6)	0.0047(6)	−0.0002(5)	0.0001(4)	−0.0001(5)
Si2	8*i*	0.65113(13)	0.35632(12)	0.36481(12)	1	0.0051(3)	0.0052(6)	0.0052(6)	0.0049(6)	−0.0002(5)	0.0002(5)	0.0011(5)
Si3	4*g*	0.78242(19)	0.11189(16)	0	1	0.0052(4)	0.0068(9)	0.0051(8)	0.0036(8)	0	0	−0.0002(7)
N1	8*i*	0.8346(4)	0.1834(4)	−0.1228(4)	1	0.0071(8)	0.010(2)	0.0051(17)	0.0059(19)	−0.0011(15)	0.0014(15)	−0.0013(15)
N2	8*i*	1.0218(4)	0.1940(4)	0.2892(4)	1	0.0088(8)	0.008(2)	0.0064(18)	0.012(2)	0.0022(16)	−0.0031(16)	0.0010(15)
N3	8*i*	0.7697(4)	0.2533(4)	0.3502(3)	1	0.0056(7)	0.0061(19)	0.0057(17)	0.0051(17)	0.0001(15)	0.0025(14)	0.0000(15)
N4	4*h*	0.6041(6)	0.3920(6)	$\frac{1}{2}$	1	0.0080(12)	0.007(3)	0.013(3)	0.004(3)	0	0	0.005(2)
N5	8*i*	0.6817(4)	0.4901(3)	0.3090(3)	0.25	0.0070(7)	0.0073(16)	0.0062(16)	0.0074(16)	0.0032(13)	−0.0001(13)	−0.0014(13)
O5					0.75							
N6	8*i*	0.9171(4)	0.3957(3)	0.2048(3)	0.25	0.0059(7)	0.0061(17)	0.0064(16)	0.0051(16)	0.0005(13)	−0.0007(14)	−0.0001(13)
O6					0.75							
N7	4*g*	0.8498(5)	−0.0249(5)	0	0.25	0.0091(10)	0.012(3)	0.010(2)	0.005(2)	0	0	0.001(2)
O7					0.75							
N8	4*g*	0.6228(6)	0.0916(6)	0	0.25	0.0150(12)	0.015(3)	0.016(3)	0.014(3)	0	0	0.001(2)
O8					0.75							
Br1	4*h*	0.5375(3)	0.0270(2)	$\frac{1}{2}$	0.492(6)	0.0423(10)	0.058(2)	0.0490(18)	0.0200(11)	0	0	0.0213(12)
Nd1	8*i*	0.642553(18)	0.102941(18)	0.23372(2)	1	0.00533(8)	0.00349(11)	0.00445(11)	0.00751(14)	−0.00091(7)	−0.00030(7)	−0.00007(6)
Nd2	4*h*	0.87129(3)	0.11979(3)	$\frac{1}{2}$	1	0.00771(9)	0.00914(14)	0.00772(14)	0.00626(18)	0	0	0.00349(9)
Nd3	4*e*	1	0	0.16675(3)	1	0.00574(8)	0.00671(13)	0.00548(13)	0.00502(17)	0	0	0.00109(9)
Nd4	4*g*	0.61370(3)	−0.12753(3)	0	1	0.00874(9)	0.01785(16)	0.00468(14)	0.00370(18)	0	0	0.00205(10)
Si1	8*i*	0.88506(9)	0.25752(9)	0.24611(10)	1	0.0035(2)	0.0034(4)	0.0043(5)	0.0027(6)	−0.0000(3)	−0.0001(3)	−0.0003(3)
Si2	8*i*	0.65170(9)	0.35605(8)	0.36467(10)	1	0.0035(2)	0.0033(4)	0.0041(4)	0.0031(6)	−0.0003(4)	0.0000(3)	0.0005(3)

Si3	4*g*	0.78224(13)	0.11056(12)	0	1	0.0039(3)	0.0048(6)	0.0047(6)	0.0021(8)	0	0	−0.0009(5)
N1	8*i*	0.8335(3)	0.1833(3)	−0.1227(3)	1	0.0063(6)	0.0077(13)	0.0078(13)	0.0034(17)	0.0014(12)	0.0015(11)	0.0000(11)
N2	8*i*	1.0253(3)	0.1939(3)	0.2840(3)	1	0.0077(6)	0.0070(14)	0.0062(13)	0.0100(19)	−0.0013(12)	−0.0041(12)	0.0023(11)
N3	8*i*	0.7710(3)	0.2512(3)	0.3521(3)	1	0.0044(6)	0.0040(12)	0.0045(12)	0.0047(17)	−0.005(11)	0.0006(10)	−0.0002(10)
N4	4*h*	0.6008(5)	0.3891(4)	$\frac{1}{2}$	1	0.0078(9)	0.011(2)	0.011(2)	0.002(3)	0	0	0.0017(16)
N5	8*i*	0.6822(3)	0.4923(2)	0.3108(3)	0.25	0.0060(5)	0.0070(12)	0.0043(11)	0.0066(16)	0.0007(10)	0.0000(10)	0.0001(9)
O5					0.75							
N6	8*i*	0.9166(3)	0.3980(2)	0.2041(3)	0.25	0.0048(5)	0.0049(12)	0.0047(11)	0.0048(16)	−0.0003(9)	0.0003(10)	0.0000(9)
O6					0.75							
N7	4*g*	0.8517(4)	−0.0276(4)	0	0.25	0.0079(8)	0.0125(19)	0.0067(18)	0.004(2)	0	0	0.0000(14)
O7					0.75							
N8	4*g*	0.6207(4)	0.0910(4)	0	0.25	0.0159(10)	0.0077(18)	0.018(2)	0.022(3)	0	0	−0.0013(15)
O8					0.75							
Br1	4*h*	0.54130(18)	0.02938(16)	$\frac{1}{2}$	0.495(4)	0.0360(6)	0.0473(11)	0.0409(11)	0.0198(11)	0	0	0.0180(7)
Nd1	8*i*	0.643253(19)	0.103366(19)	0.234124(18)	1	0.00592(6)	0.00336(10)	0.00354(10)	0.01086(11)	−0.00133(7)	−0.00046(7)	−0.00001(7)
Nd2	4*h*	0.87075(3)	0.11974(3)	$\frac{1}{2}$	1	0.00853(7)	0.00617(13)	0.00718(14)	0.00680(13)	0	0	0.00444(11)
Nd3	4*e*	1	0	0.16699(2)	1	0.00542(7)	0.00617(13)	0.00465(12)	0.00544(12)	0	0	0.00106(10)
Nd4	4*g*	0.61378(3)	−0.12711(3)	0	1	0.00874(7)	0.01831(16)	0.00371(13)	0.00420(13)	0	0	0.00250(10)
Si1	8*i*	0.88558(9)	0.25806(9)	0.24618(8)	1	0.00326(18)	0.0024(4)	0.0036(5)	0.0038(4)	−0.0002(3)	−0.0003(3)	0.0002(3)
Si2	8*i*	0.65185(10)	0.35644(9)	0.36474(9)	1	0.00328(18)	0.0023(4)	0.0036(4)	0.0039(4)	−0.0002(3)	0.0000(4)	0.0002(3)
Si3	4*g*	0.78268(14)	0.11096(13)	0	1	0.0037(3)	0.0045(6)	0.0032(6)	0.0034(6)	0	0	−0.0014(5)
N1	8*i*	0.8342(3)	0.1842(3)	−0.1228(3)	1	0.0059(6)	0.0063(14)	0.0070(14)	0.0044(13)	0.0007(12)	0.0002(17)	−0.0020(11)
N2	8*i*	1.0257(3)	0.1946(3)	0.2837(3)	1	0.0082(6)	0.0061(14)	0.0069(14)	0.0116(15)	−0.0007(12)	−0.0039(12)	−0.0004(11)
N3	8*i*	0.7721(3)	0.2521(3)	0.3521(3)	1	0.0043(6)	0.0051(4)	0.0031(13)	0.0049(13)	0.0005(10)	−0.0004(11)	0.0010(11)
N4	4*h*	0.6008(5)	0.3898(4)	$\frac{1}{2}$	1	0.0074(9)	0.007(2)	0.010(2)	0.005(2)	0	0	0.0069(17)
N5	8*i*	0.6820(3)	0.4922(3)	0.3100(2)	0.25	0.0063(5)	0.0060(12)	0.0040(12)	0.0089(13)	0.0014(10)	−0.0012(10)	−0.0001(10)
O5					0.75							
N6	8*i*	0.9175(3)	0.3984(2)	0.2047(2)	0.25	0.0043(5)	0.0049(12)	0.0034(12)	0.0046(12)	0.0008(10)	0.0008(10)	0.0003(10)
O6					0.75							
N7	4*g*	0.8516(4)	−0.0259(4)	0	0.25	0.0071(8)	0.0090(19)	0.0072(19)	0.0050(17)	0	0	0.0025(15)
O7					0.75							
N8	4*g*	0.6209(4)	0.0910(5)	0	0.25	0.0155(10)	0.010(2)	0.015(2)	0.021(2)	0	0	0.0015(17)
O8					0.75							
Cl1	4*h*	0.5755(4)	0.0493(3)	$\frac{1}{2}$	0.482(9)	0.0224(11)	0.0234(19)	0.0263(19)	0.0174(18)	0	0	0.0010(14)

U_{eq} is defined as one third of the trace of the U_{ij} tensor. The anisotropic displacement factor exponent is of the form $-2\pi^2[(ha*)^2U_{11}+\ldots 2hka*b*U_{12}]$.

Table 3
Selected interatomic distances (Å) and angles (°) in the structure of $Ce_{10}[Si_{10}O_9N_{17}]Br$, $Nd_{10}[Si_{10}O_9N_{17}]Br$ and $Nd_{10}[Si_{10}O_9N_{17}]Cl$ determined by single-crystal X-ray diffraction with standard deviations in parentheses

$Ce_{10}[Si_{10}O_9N_{17}]Br$							
Ce1–O/N5	2.409(4)	Ce2–N4	2.447(7)	Ce3–O/N7 (2 ×)	2.531(4)	Ce4–O/N6(2 ×)	2.420(4)
Ce1–O/N6	2.419(4)	Ce2–N3 (2 ×)	2.530(4)	Ce3–O/N5 (2 ×)	2.538(4)	Ce4–O/N8	2.459(7)
Ce1–O/N6	2.431(4)	Ce2–N4	2.607(7)	Ce3–N2 (2 ×)	2.609(4)	Ce4–O/N8	2.560(7)
Ce1–N3	2.547(4)	Ce2–O/N5	2.742(4)	Ce3–N1 (2 ×)	2.755(4)	Ce4–N1(2 ×)	2.616(4)
Ce1–N1	2.588(4)	Ce2–O/N5	2.742(4)			Ce4–O/N7	2.739(6)
Ce1–N2	2.697(4)	Ce2–N2 (2 ×)	3.016(5)				
Ce1–O/N8	2.7465(7)	Ce2–Br1	3.732(3)	Br1–Br1[a]	1.000(6)		
Ce1–Br1	3.3814(13)						
Si1–O/N6	1.664(4)	Si2–O/N5	1.668(4)	Si3–O/N7	1.695(6)		
Si1–N2	1.693(4)	Si2–N4	1.697(3)	Si3–O/N8	1.709(7)		
Si1–N3	1.715(4)	Si2–N3	1.718(4)	Si3–N1 (2 ×)	1.729(4)		
Si1–N1	1.745(4)	Si2–N2	1.726(4)				
O/N6–Si1–N2	107.5(2)	O/N5–Si2–N4	101.8(3)	O/N7–Si3–N8	107.3(3)	Si3–N1–Si1	178.9(3)
O/N6–Si1–N3	112.1(2)	O/N5–Si2–N3	115.2(2)	O/N7–Si3–N1 (2 ×)	106.60(18)	Si1–N2–Si2	166.0(3)
N2–Si1–N3	113.2(2)	N4–Si2–N3	117.8(2)	O/N8–Si3–N1 (2 ×)	112.29(19)	Si1–N3–Si2	125.0(2)
O/N6–Si1–N1	105.5(2)	O/N5–Si2–N2	104.5(2)	N1–Si3–N1	111.3(3)	Si2–N4–Si2	135.7(4)
N2–Si1–N1	107.6(2)	N4–Si2–N2	108.4(3)				
N3–Si1–N1	110.5(2)	N3–Si2–N2	108.2(2)				
$Nd_{10}[Si_{10}O_9N_{17}]Br$							
Nd1–O/N6	2.383(3)	Nd2–N4	2.417(5)	Nd3–O/N7 (2 ×)	2.497(3)	Nd4–O/N6(2 ×)	2.396(3)
Nd1–O/N5	2.388(3)	Nd2–N3 (2 ×)	2.481(3)	Nd3–O/N5 (2 ×)	2.540(3)	Nd4–O/N8	2.427(5)
Nd1–O/N6	2.402(3)	Nd2–N4	2.578(5)	Nd3–N2 (2 ×)	2.556(3)	Nd4–O/N8	2.500(5)
Nd1–N3	2.531(3)	Nd2–O/N5	2.663(3)	Nd3–N1 (2 ×)	2.733(3)	Nd4–N1(2 ×)	2.593(3)
Nd1–N1	2.545(3)	Nd2–O/N5	2.663(3)			Nd4–O/N7	2.739(4)
Nd1–N2	2.636(3)	Nd2–N2 (2 ×)	3.0863(3)	Br1–Br1[a]	1.087(4)		
Nd1–O/N8	2.7117(7)	Nd2–Br1	3.615(2)				
Nd1–Br1	3.3548(10)						
Si1–O/N6	1.667(3)	Si2–O/N5	1.666(3)	Si3–O/N7	1.699(4)		
Si1–N2	1.694(3)	Si2–N4	1.692(2)	Si3–O/N8	1.713(5)		
Si1–N3	1.715(3)	Si2–N2	1.716(3)	Si3–N1 (2 ×)	1.718(3)		
Si1–N1	1.733(4)	Si2–N3	1.718(3)				
O/N6–Si1–N2	106.98(16)	O/N5–Si2–N4	102.0(2)	O/N7–Si3–N8	108.2(2)	Si3–N1–Si1	179.7(2)
O/N6–Si1–N3	112.64(15)	O/N5–Si2–N3	116.27(15)	O/N7–Si3–N1 (2 ×)	106.82(14)	Si1–N2–Si2	161.9(2)
N2–Si1–N3	114.08(17)	N4–Si2–N3	117.1(2)	O/N8–Si3–N1 (2 ×)	111.80(14)	Si1–N3–Si2	122.95(19)
O/N6–Si1–N1	105.54(16)	O/N5–Si2–N2	103.88(16)	N1–Si3–N1	111.1(2)	Si2–N4–Si2	134.9(3)
N2–Si1–N1	106.67(16)	N4–Si2–N2	109.0(2)				
N3–Si1–N1	110.39(16)	N3–Si2–N2	107.59(16)				
$Nd_{10}[Si_{10}O_9N_{17}]Cl$							
Nd1–O/N5	2.383(3)	Nd2–N4	2.425(5)	Nd3–O/N7 (2 ×)	2.498(3)	Nd4–O/N6(2 ×)	2.402(3)
Nd1–O/N6	2.390(3)	Nd2–N3 (2 ×)	2.481(3)	Nd3–O/N5 (2 ×)	2.532(3)	Nd4–O/N8	2.424(5)
Nd1–O/N6	2.402(3)	Nd2–N4	2.572(5)	Nd3–N2 (2 ×)	2.562(3)	Nd4–O/N8	2.505(5)
Nd1–N3	2.535(3)	Nd2–O/N5	2.669(3)	Nd3–N1 (2 ×)	2.738(3)	Nd4–N1(2 ×)	2.589(3)
Nd1–N1	2.550(3)	Nd2–O/N5	2.669(3)			Nd4–O/N7	2.746(4)
Nd1–N2	2.626(3)	Nd2–N2 (2 ×)	3.097(3)	Cl1–Cl1[a]	1.931(8)		
Nd1–O/N8	2.7161(8)	Nd2–Cl1	3.207(4)				
Nd1–Cl1	3.208(1)						
Si1–O/N6	1.665(3)	Si2–O/N5	1.666(3)	Si3–O/N7	1.685(4)		
Si1–N2	1.692(3)	Si2–N4	1.693(2)	Si3–O/N8	1.718(5)		
Si1–N3	1.711(3)	Si2–N2	1.721(3)	Si3–N1 (2 ×)	1.721(3)		
Si1–N1	1.731(3)	Si2–N3	1.723(3)				
O/N6–Si1–N2	106.69(16)	O/N5–Si2–N4	102.2(2)	O/N7–Si3–N8	108.1(2)	Si3–N1–Si1	179.8(3)
O/N6–Si1–N3	112.52(15)	O/N5–Si2–N3	115.90(15)	O/N7–Si3–N1 (2 ×)	106.88(14)	Si1–N2–Si2	161.8(2)
N2–Si1–N3	114.22(16)	N4–Si2–N3	117.34(18)	O/N8–Si3–N1 (2 ×)	111.94(14)	Si1–N3–Si2	123.21(18)
O/N6–Si1–N1	105.70(15)	O/N5–Si2–N2	103.88(16)	N1–Si3–N1	110.8(2)	Si2–N4–Si2	134.6(3)
N2–Si1–N1	106.62(17)	N4–Si2–N2	109.1(2)				
N3–Si1–N1	110.57(16)	N3–Si2–N2	107.44(16)				

[a]Distance between symmetrically equivalent split positions.

Table 4
Crystallographic data and details of the powder X-ray data collection for $Ce_{10}[Si_{10}O_9N_{17}]Br$, $Nd_{10}[Si_{10}O_9N_{17}]Br$ and $Nd_{10}[Si_{10}O_9N_{17}]Cl$

Lanthanide element, halide anion	Ce, Br	Nd, Br	Nd, Cl
Diffractometer		STOE Stadi P	
Monochromator		Germanium	
Radiation		MoK_α ($\lambda = 0.7093$ Å)	
Temperature/K		293(2)	
Sample container		Glass capillary	
Background		Fixed	
Diffraction range/°	$3<2\theta<60$	$2<2\theta<60$	$2<2\theta<60$
Observed reflections	2114	2061	2114
Refined parameters	53	53	56
R_{F^2}	0.12808	0.11643	0.0713
$R_{p(fit)}$	0.0671	0.0431	0.0451
$wR_{p(fit)}$	0.0916	0.0559	0.0585
$R_{p(back)}$	0.0766	0.0460	0.0422
$wR_{p(back)}$	0.1071	0.0621	0.0528
Red. χ^2	5.525	2.266	1.795
Lattice parameters, a/Å	10.5988(12)	10.5072(4)	10.5169(3)
b/Å	11.2115(13)	11.0835(4)	11.0940(3)
c/Å	11.5969(13)	11.5344(4)	11.5249(3)
Cell volume, V/Å^3	1378.1(3)	1343.2(1)	1344.66(7)

Lattice parameters were determined using GSAS.

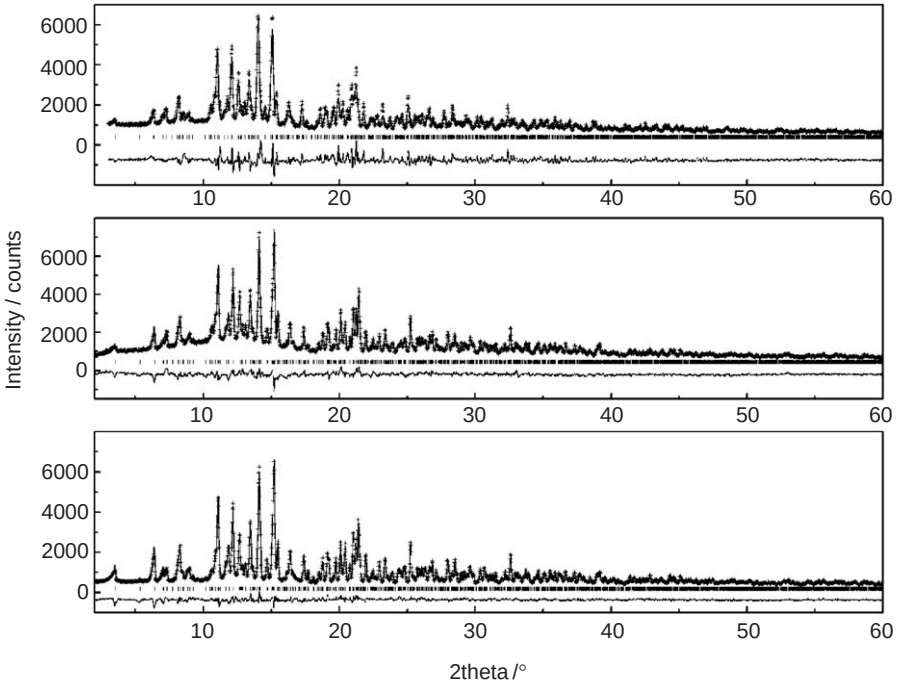

Fig. 1. Rietveld profile fits of the X-ray powder diffraction data of $Ce_{10}[Si_{10}O_9N_{17}]Br$, $Nd_{10}[Si_{10}O_9N_{17}]Br$ and $Nd_{10}[Si_{10}O_9N_{17}]Cl$ ($MoK_\alpha = 0.71730$ Å, $2\theta = 2$ resp. 3–60°). Observed (crosses) and calculated (line) diffractograms as well as the difference profile (lower line). The row of vertical lines indicates the possible reflection positions. Top: $Ce_{10}[Si_{10}O_9N_{17}]Br$, middle: $Nd_{10}[Si_{10}O_9N_{17}]Br$, bottom: $Nd_{10}[Si_{10}O_9N_{17}]Cl$.

Table 5
Results of the chemical analyses (all values given in weight%) of $Nd_{10}[Si_{10}O_9N_{17}]Br$

	Nd	Si	O	N	Br	Total
Measured	65.6/65.9	13.0/12.9	6.8/7.2	11.2/11.3	3.55/3.54	
Average	65.8	13.0	7.0	11.3	3.55	100.65
Calculated	66.0	12.9	6.6	10.9	3.66	100

Table 6
Parameters of the EPMA measurements

Element, X-ray line	Standard	Spectrometer crystal	Measuring time on peak (s)	Measuring time on background (s)
Ce, *Lα*	$Ce_3Si_6N_{11}$ [10]	PET	90	45+45
Nd, *Lα*	$NdPO_4$ [36]	PET	60	45+45
Si, *Kα*	$Ce_3Si_6N_{11}$	TAP	90	90
N, *Kα*	$Ce_3Si_6N_{11}$	LDE1	120	60+60
O, *Kα*	Albite [37]	LDE1	40	40
Cl, *Kα*	Scapolite [38]	PETH	180	90+90
Br, *Lα*	KBr	TAP	60	30+30

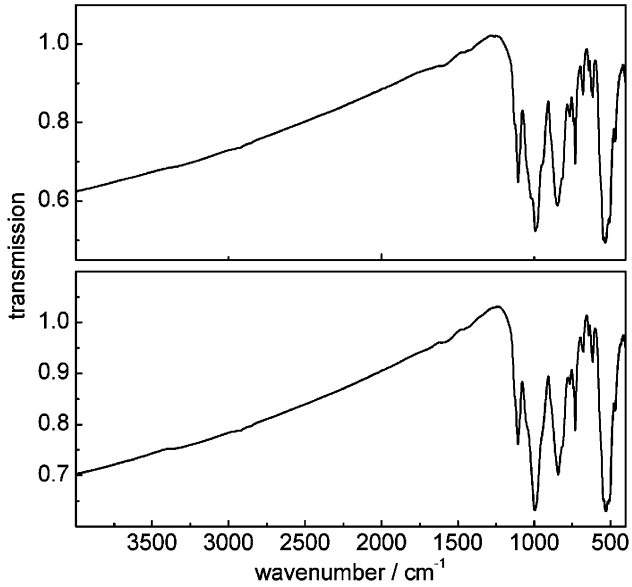

Fig. 2. FTIR spectra of $Nd_{10}[Si_{10}O_9N_{17}]Br$ (top) and $Nd_{10}[Si_{10}O_9N_{17}]Cl$ (bottom) recorded at ambient temperature. The two samples were exemplarily chosen.

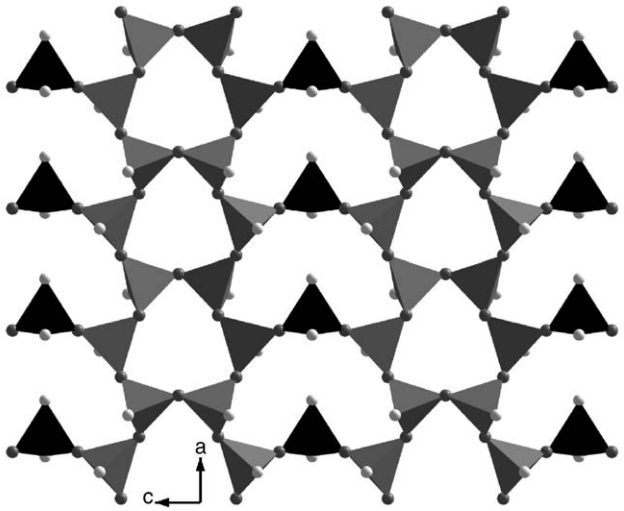

Fig. 3. Anionic layer $[Si_{10}O_9N_{17}]^{29-}$ of $Ce_{10}[Si_{10}O_9N_{17}]Br$, $Nd_{10}[Si_{10}O_9N_{17}]Br$ and $Nd_{10}[Si_{10}O_9N_{17}]Cl$. Tetrahedra of Q^3 type: light gray, tetrahedra of Q^2 type: black, N: medium gray spheres, mixed O/N: white spheres. View along [010].

Table 7
Quantitative results of the EPMA analyses

		Ce	Nd	Si	O	N	Br	Cl	Total	No. of spots
$Ce_{10}[Si_{10}O_9N_{17}]Br$										30
Wt.%	Average	67.12	0	13.30	6.62	11.34	3.96	0	102.36	
	1 sigma	0.14	0	0.07	0.10	0.24	0.03	0		
Atom. rat.	Average	21.52	0	21.30	18.59	36.35	2.22	0		
	1 sigma	0.12	0	0.21	0.35	0.58	0.02	0		
Stoichiom. formula		10.05		9.95	8.68	16.98	1.04		46.71	
$Nd_{10}[Si_{10}O_9N_{17}]Br$										29
Wt.%	Average	0	66.23	13.22	6.86	11.35	3.69	0	101.57	
	1 sigma	0	0.16	0.07	0.12	0.36	0.03	0		
Atom. rat.	Average	0	20.69	21.20	19.31	36.50	2.08	0		
	1 sigma	0	0.21	0.25	0.46	0.85	0.02	0		
Stoichiom. formula			9.80	10.05	9.15	17.30	0.99		47.39	
$Nd_{10}[Si_{10}O_9N_{17}]Cl$										24
Wt.%	Average	0	67.51	13.10	7.12	11.59	0	2.06	101.44	
	1 sigma	0	0.13	0.10	0.17	0.30	0	0.01		
Atom. rat.	Average	0	20.67	20.59	19.63	36.52	0	2.56		
	1 sigma	0	0.12	0.21	0.51	0.77	0	0.02		
Stoichiom. formula			10.02	9.98	9.52	17.70		1.24	48.47	

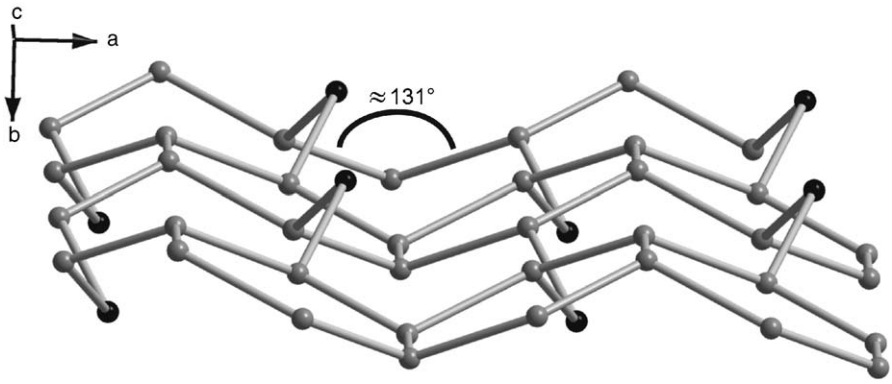

Fig. 4. Topological view of the anionic layer $[Si_{10}O_9N_{17}]^{29-}$. Notice the almost planar 6 rings and the interconnecting atoms above and below the layer. Si of Q^3 tetrahedra: light gray, Si of Q^2 tetrahedra: black.

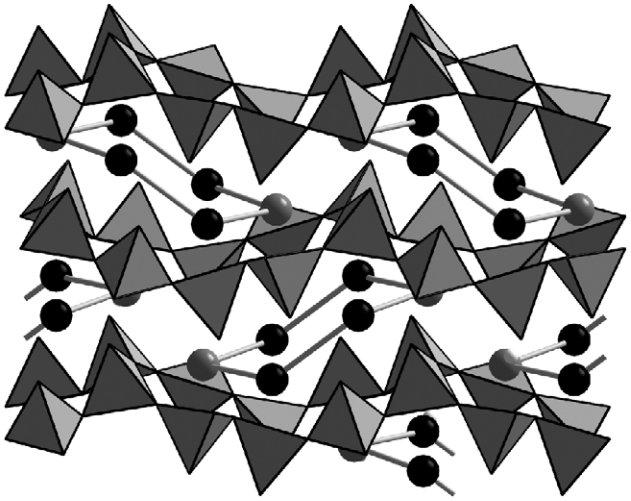

Fig. 5. Six-membered rings of *Ln*1 and *Ln*2 atoms and their position between the oxonitridosilicate layers. *Ln*3 and *Ln*4 are omited. *Ln*1: black spheres, *Ln*2: gray spheres. View along [001].

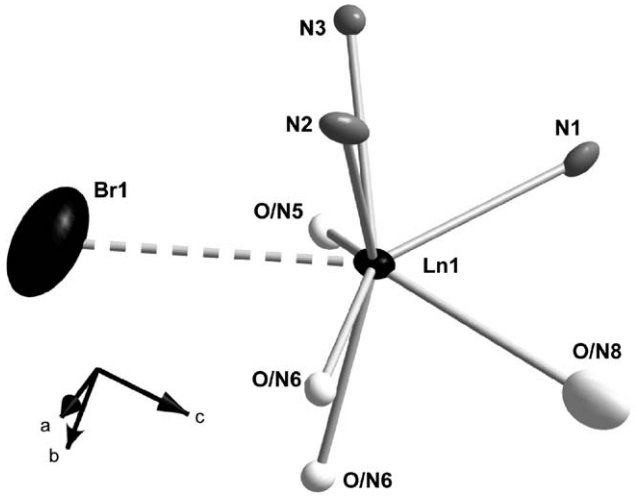

Fig. 6. Coordination sphere of the lanthanide *Ln*1. $Nd_{10}[Si_{10}O_9N_{17}]Br$ has been exemplarily chosen. Displacement ellipsoids are drawn at the 90% probability level.

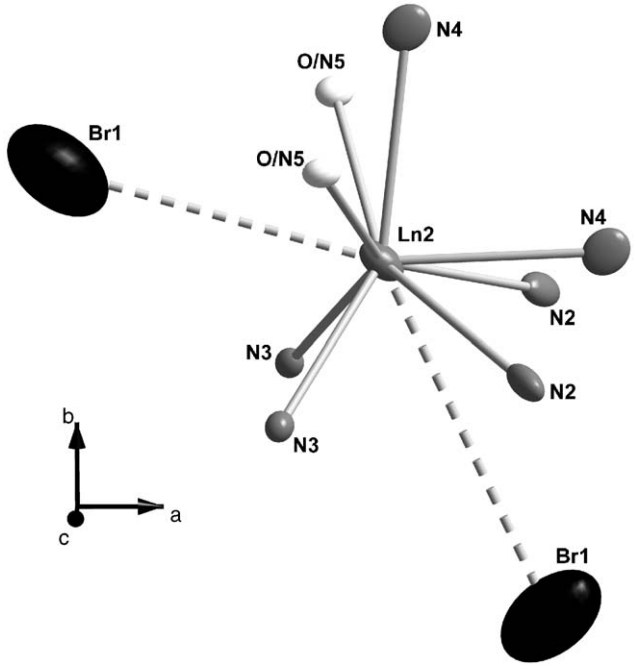

Fig. 7. Coordination sphere of the lanthanide *Ln*2. $Nd_{10}[Si_{10}O_9N_{17}]Br$ has been exemplarily chosen. Displacement ellipsoids are drawn at the 90% probability level.

crystals. The totals of the analyses vary between 101.4% and 102.4%, thus indicating a good quality of the analysis of light elements in a difficult matrix. The resulting elemental compositions agree well with the theoretical values for all elements, deriving from the empirical formula extracted from single-crystal X-ray data (Table 7).

3.2. Crystal structure

Only very few nitridosilicates and oxonitridosilicates with layered structures have yet been found owing to the high tendency of nitrogen to build three-dimensional networks [22–25]. There are only five layered structure types in nitrogen containing silicate and aluminosilicate

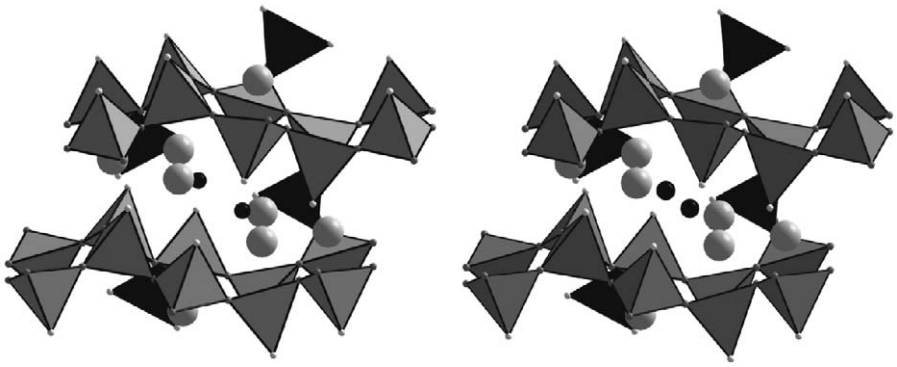

Fig. 8. $Nd_{10}[Si_{10}O_9N_{17}]Cl$ (left) and $Nd_{10}[Si_{10}O_9N_{17}]Br$ (right): possible positions of the respective halide anions (split position with an occupancy factor of 0.5). Nd: large gray spheres, halide: small black spheres, N: small medium gray spheres, mixed O/N: small white spheres. View along [001].

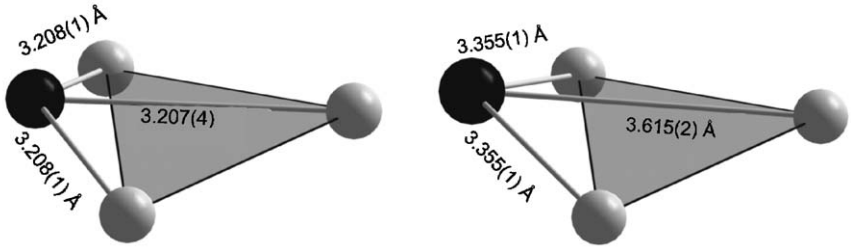

Fig. 9. $Nd_{10}[Si_{10}O_9N_{17}]Cl$ (left) and $Nd_{10}[Si_{10}O_9N_{17}]Br$ (right): assumed coordination sphere of the respective halide anions. Nd: gray spheres, halide: black spheres.

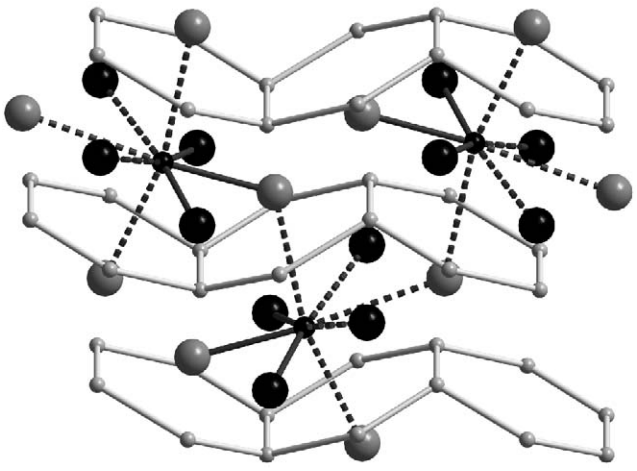

Fig. 10. Topological representation of the tetrahedra layer and surrounding of the halide anions (*Ln*1 and *Ln*2 cations). The occupation of the halide position has been selected statistically. *Ln*1: large black spheres, *Ln*2: large gray spheres, halide: small black spheres, Si: small light gray spheres.

systems, like $MSiN_2$ with $M = Sr$, Ba [26] with puckered layers composed of pairs of edge-sharing tetrahedra joined at their remaining vertices, $Ln_2Si_3O_3N_4$ with $Ln = Y$, La, Ce, Nd, Sm, Gd, Dy, Ho, Er, Yb [14,15] and $Ln_2Si_{2.5}Al_{0.5}O_{3.5}N_{3.5}$ with $Ln = Ce$, Pr, Nd, Sm, Gd [27] (melilite phases) showing planar layers consisting solely of five-membered tetrahedra rings, $Ce_4[Si_4O_4N_6]O$ [28] / $Ln_4[Si_4O_{3+x}N_{7-x}]Cl_{1-x}O_x$ with $Ln = Ce$, Pr, Nd and $x \approx 0.2$ [7] with a hyperbolically corrugated layer and complex cations $[Ln_4(O_x/Cl_{1-x})]^{+12-(1+x)}$, $Ca[Si_2O_2N_2]$ [29] with layers similar to sinoite Si_2N_2O [30] with intercalated cations and $Sr_{10}Sm_6[Si_{30}Al_6O_7N_{54}]$ made up of double layers [31].

The title compounds $Ce_{10}[Si_{10}O_9N_{17}]Br$, $Nd_{10}[Si_{10}O_9N_{17}]Br$ and $Nd_{10}[Si_{10}O_9N_{17}]Cl$ are isotypic and represent a new layered structure type. $Nd_{10}[Si_{10}O_9N_{17}]Br$ and $Nd_{10}[Si_{10}O_9N_{17}]Cl$ show almost the same cell parameters. $Ce_{10}[Si_{10}O_9N_{17}]Br$ exhibits a slightly larger cell owing to the larger Ce^{3+} ions (Table 1), whereas *b* is most elongated because it is perpendicular to the anionic $Si(O/N)_4$-tetrahedra layers and to the formfitting six-membered rings of lanthanide ions between them.

The oxonitridosilicate compounds presented in this contribution resemble classical oxosilicates as only doubly bridging and terminal O and N atoms occur and all tetrahedra are connected through their corners. However, the topology of their layers is unprecedented in the oxosilicate class of compounds: The anionic layers $[Si_{10}O_9N_{17}]^{29-}$ (Fig. 3) are made up of $[SiN_2(O/N)_2]$ and $[SiN_3(O/N)]$ units representing Q^2 and Q^3 type tetrahedra. The molar ratio of the tetrahedra Q^2:Q^3 is 1:4, giving a less dense layer structure than e.g. $Ce_4[Si_4O_4N_6]O$ [28] which solely consists of Q^3 tetrahedra. The atomic ratio Si:*X* with $X = O$, N is 2:5.2. This value perfectly fits into the known range of condensation degrees from open- and loop-

Table 8
Environment of the halide anion represented by selected interatomic distances (Å) in the structure of $Ce_{10}[Si_{10}O_9N_{17}]Br$, $Nd_{10}[Si_{10}O_9N_{17}]Br$ and $Nd_{10}[Si_{10}O_9N_{17}]Cl$ determined by single-crystal X-ray diffraction with standard deviations in parentheses

$Ce_{10}[Si_{10}O_9N_{17}]Br$			$Nd_{10}[Si_{10}O_9N_{17}]Br$			$Nd_{10}[Si_{10}O_9N_{17}]Cl$		
Ce1	3.381(1)	2 ×	Nd1	3.355(1)	2 ×	Nd1	3.208(1)	2 ×
Ce2	3.732(3)		Nd2	3.615(2)		Nd2	3.207(4)	
Ce1	3.903(2)	2 ×	Nd1	3.918(1)	2 ×	Nd1	4.196(3)	2 ×
Ce2	4.295(2)		Nd2	4.286(2)		Nd2	4.263(4)	
Ce2	4.632(2)		Nd2	4.639(2)		Nd2	4.805(3)	
Ce2	4.682(2)		Nd2	4.647(2)		Nd2	5.062(4)	
(O/N)5	3.740(5)	2 ×	(O/N)5	3.662(5)	2 ×	(O/N)5	3.426(4)	2 ×
(O/N)6	3.764(4)	2 ×	(O/N)6	3.741(3)	2 ×	N3	3.504(5)	2 ×
(O/N)6	3.767(4)	2 ×	(O/N)6	3.748(4)	2 ×	N4	3.792(6)	
N3	3.945(5)	2 ×	N3	3.850(4)	2 ×	(O/N)6	3.799(3)	2 ×
N2	3.982(5)	2 ×	N2	3.960(4)	2 ×	N2	3.821(4)	2 ×
						Si2	3.837(3)	2 ×
						(O/N)6	3.838(3)	2 ×

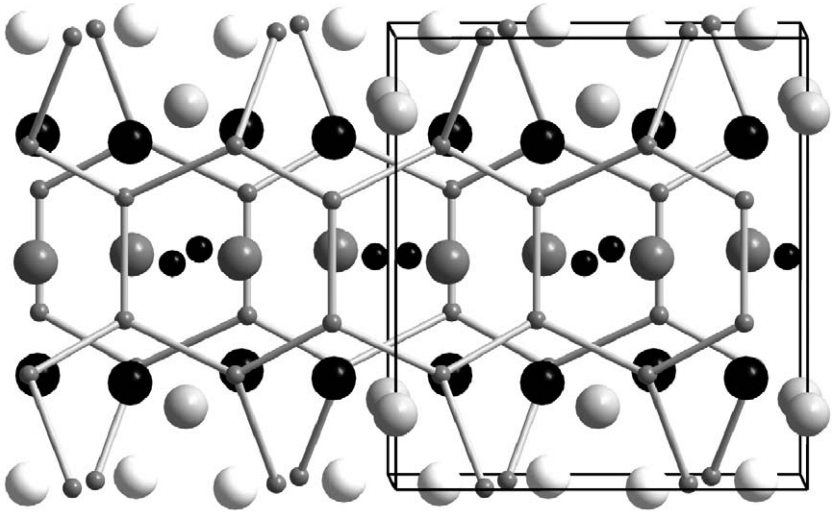

Fig. 11. Overview over the different crystallographic sites of the *Ln* atoms. The figure shows the possible symmetrically equivalent positions of the halide anions (the site occupancy factor is 0.5). *Ln*3 and *Ln*4 are far away from the halide anions and do not take part in their coordination spheres. Si: small medium gray spheres, halide: small black spheres, *Ln*1: large black spheres, *Ln*2: large medium gray spheres, *Ln*3: large light gray spheres, *Ln*4: large white spheres. View along [010].

branched silicate single layers, ranging from 2:4.67 ($NaPr[Si_6O_{14}]$) to 2:5.71 (meliphanite) [32].

According to *Liebau* the $[Si_{10}O_9N_{17}]^{29-}$ layer of the title compounds has to be specified as an open-branched vierer single chain layer [31–34]. The resulting formula is $Ln_{10}\{oB, 1^2_\infty\}[^4Si_{10}O_9N_{17}]X$. Another structure interpretation leads to double chains of almost planar sechser rings built up by Q^3 tetrahedra. These rings are interconnected by Q^2 tetrahedra resulting in additional achter rings (Fig. 4). The double chains are slightly corrugated showing an angle of about 131° (Ce/Br: 131.53(1)°, Nd/Br: 131.78(1)°, Nd/Cl: 131.64(1)°) enclosed by the sechser rings. The interconnecting tetrahedra can be found alternately above and below these double chains. Along [010] the stacking sequence is ABAB, wherein every second layer is rotated 180°. The distance between two equivalent layers equals the length of *b*.

The lanthanide ions are located on four different crystallographic sites. *Ln*1 and *Ln*2 form six-membered rings in chair conformation situated between the six-membered tetrahedra rings of the silicate layers (Fig. 5). These cations are coordinated by O, N and the halide ions (Figs. 6 and 7).

The halide ions are statistically disordered on two neighboring and symmetrically equivalent positions in the center of the *Ln*1/*Ln*2-rings. The distance between the two positions shortens depending on the increasing dimension of the halide atoms (Nd/Cl: 1.931(8), Nd/Br: 1.087(4) and Ce/Br: 1.000(6) Å). Due to the split position (occupancy factor = 0.5) only one of them is present at a time. The halide ion has three shorter and five longer distances to the surrounding lanthanide cations and it is therefore assumed to be predominantly coordinated by three lanthanide atoms forming a decentered trigonal coordination sphere

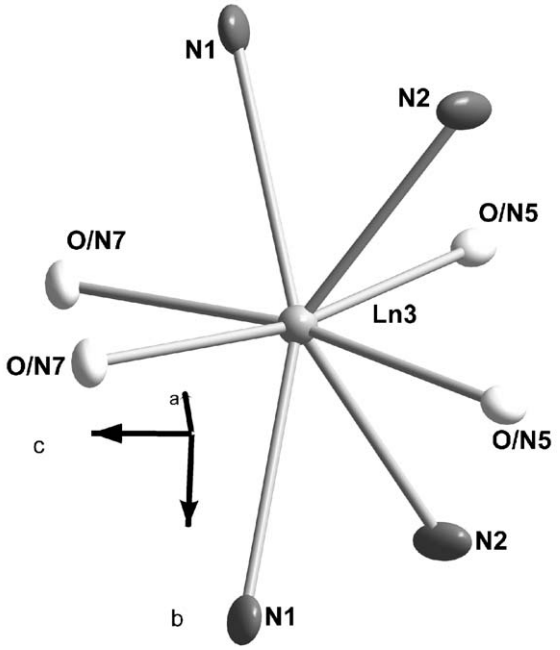

Fig. 12. Coordination sphere of the lanthanide *Ln*3. $Nd_{10}[Si_{10}O_9N_{17}]Br$ has been exemplarily chosen. Displacement ellipsoids are drawn at the 90% probability level.

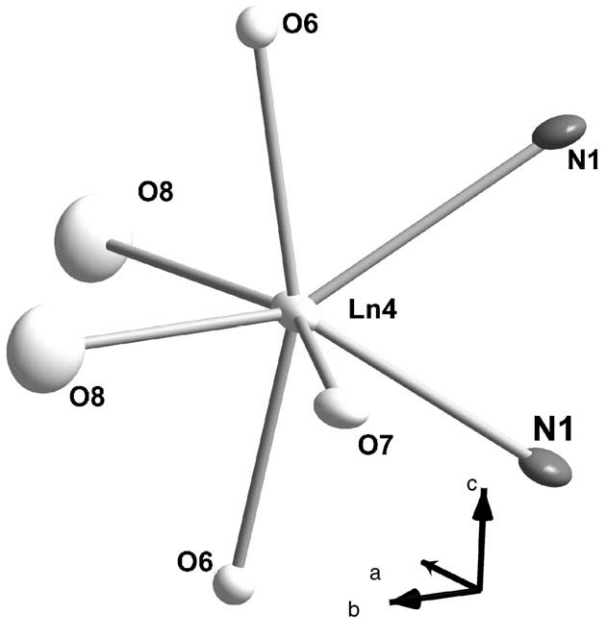

Fig. 13. Coordination sphere of the lanthanide *Ln*4. $Nd_{10}[Si_{10}O_9N_{17}]Br$ has been exemplarily chosen. Displacement ellipsoids are drawn at the 90% probability level.

(Figs. 8 and 9). Since several anions (O, N) are located between the three closer and the five more distant lanthanides, the threefold coordination of the halide atoms is more likely than an enlarged cationic coordination sphere. A similar threefold coordination of halide atoms has already been found in lanthanide oxosilicate chlorides, e.g. $Tb_3Cl_5[SiO_4]$ [35]. The five additional cations found in more distant positions are indicated with dashed lines in Fig. 10. The interatomic distances between the respective halide atoms and their surrounding atoms are listed in Table 8.

*Ln*3 and *Ln*4 are situated closer to the interconnecting $[SiN_2(O/N)_2]$ Q^2 type tetrahedra and do not participate in the coordination of the halide ions (Fig. 11). *Ln*3 and *Ln*4 are solely coordinated by O and N (Figs. 12 and 13).

4. Conclusions

The title compounds represent three new members in the class of oxonitridosilicate halides. They extend the very large field of classical layered oxosilicate structures by showing a new topology of the tetrahedra layer. This may derive from the integration of nitrogen and halides in the oxosilicate system, which will be subject of further investigations. For the first time, bromide could be implanted in oxonitridosilicates. The existence of the isotypic chlorine compound shows the possibility for halide substitution in the oxonitridosilicate system, which leads to an interesting field for further scientific work. The characterization of the new oxonitridosilicate halides was carried out by means of single-crystal and powder X-ray diffraction and chemical and microprobe analyses. The formerly established method for measuring light elements by EPMA [7] could be successfully transferred to the new system.

Acknowledgments

The authors would like to thank the Deutsche Forschungsgemeinschaft (SPP 1136 "Substitutionseffekte in Festkörpern", projekt SCHN 377/9) and the Fonds der Chemischen Industrie for generous financial support. Thanks are given to Dr. Heidi E. Höfer (Department of Mineralogy, Institut for Petrology and Geochemistry, J.-W. Goethe University of Frankfurt/Main, Germany) for performing the EPMA measurements. Additional thanks go to Christoph Röhlich for sample preparation.

References

[1] W. Schnick, H. Huppertz, Chem. Eur. J. 3 (1997) 679.
[2] W. Schnick, T. Schlieper, H. Huppertz, K. Köllisch, M. Orth, R. Bettenhausen, B. Schwarze, R. Lauterbach, Phosphorus Sulfur 124/125 (1997) 163.
[3] E. Schiebold, G. Seumel, Z. Krist. 81/4 (1931) 110.
[4] C. Sieke, I. Hartenbach, T. Schleid, Z. Anorg. Allg. Chem. 626 (2000) 2235.
[5] H. Jacobsen, G. Meyer, W. Schipper, G. Blasse, Z. Anorg. Allg. Chem. 620 (1994) 451.
[6] C. Ayasse, H.A. Eick, Inorg. Chem. 12 (1973) 1140.
[7] A. Lieb, M.T. Weller, P.F. Henry, R. Niewa, R. Pöttgen, R.-D. Hoffmann, H.E. Höfer, W. Schnick, J. Solid State Chem. 178 (2005) 976.

[8] W. Schnick, H. Huppertz, R. Lauterbach, J. Mater. Chem. 9 (1999) 289.
[9] H. Lange, G. Wötting, G. Winter, Angew. Chem. Int. Ed. Engl. 30 (1991) 1579.
[10] T. Schlieper, W. Schnick, Z. Krist. 211 (1996) 254.
[11] M. Woike, W. Jeitschko, Inorg. Chem. 34 (1995) 5105.
[12] T. Schlieper, W. Schnick, Z. Anorg. Allg. Chem. 621 (1995) 1535.
[13] W. Chen, P.L. Wang, D.S. Yan, Eur. J. Solid State Inorg. Chem. 34 (1997) 871.
[14] ICDD-Datenbank PDF2, [42–176], [48–1590], [48–1860].
[15] R. Marchand, A. Jayaweera, P. Verdier, J. Lang, C. R. Seances Acad. Sci. C 283 (1976) 675.
[16] J.P. Guha, J. Mater. Sci. 15 (1980) 262.
[17] G.M. Sheldrick, SHELXS97, Program for the Solution of Crystal Structures and SHELXL97, Program for the Refinement of Crystal Structures, University of Göttingen, 1997.
[18] P.E.D. Morgan, J. Mater. Sci. 21 (1986) 4305.
[19] R.B. Von Dreele, A.C. Larson, Programm GSAS General Structure Analysis System, Los Alamos National Laboratory, Los Alamos, 2001.
[20] J.T. Armstrong, Caltech 1993, Jeol License of CITZAF Version 3.5.
[21] G.F. Bastin, H.J.M. Heijligers, Quantitative electron probe microanalysis of nitrogen, Internal Report, Eindhoven University of Technology, 1988.
[22] G.F. Bastin, H.J.M. Heijligers, Quantitative electron probe microanalysis of oxygen, Internal Report, Eindhoven University of Technology, 1989.
[23] T. Schlieper, W. Milius, W. Schnick, Z. Anorg. Allg. Chem. 621 (1995) 1380.
[24] H. Huppertz, W. Schnick, Angew. Chem. Int. Ed. Engl. 35 (1996) 1983.
[25] H. Huppertz, W. Schnick, Chem. Eur. J. 3 (1997) 249.
[26] Z.A. Gál, P.M. Mallinson, H.J. Orchard, S.J. Clarke, Inorg. Chem. 43 (2004) 3998.
[27] R. Lauterbach, W. Schnick, Z. Anorg. Allg. Chem. 625 (1999) 429.
[28] E. Irran, K. Köllisch, S. Leoni, R. Nesper, P.F. Henry, M.T. Weller, W. Schnick, Chem. Eur. J. 6 (2000) 2714.
[29] H.A. Höppe, F. Stadler, O. Oeckler, W. Schnick, Angew. Chem. Int. Ed. 43 (2004) 5540.
[30] J. Sjöberg, G. Helgesson, I. Idrestedt, Acta Crystallogr. C 47 (1991) 2438.
[31] R. Lauterbach, W. Schnick, Solid State Sci. 2 (2000) 463.
[32] F. Liebau, Structural Chemistry of Silicates, Springer, Berlin, 1985.
[33] The classification can also be determined by using the programm CRYSTANA via http://www.is.informatik.uni-kiel.de/~hjk/crystana.html which is partially based on Ref. [32].
[34] K. Goetzke, H.-J. Klein, J. Non-Cryst. Solids 127 (1991) 215.
[35] M. Petter, I. Hartenbach, T. Nikelski, T. Schleid, Z. Krist. 219 (2004) 177.
[36] E. Jarosewich, Geostandard. Newslett. 15 (1991) 397.
[37] A.V. McGuire, C.A. Francis, M. Darby Dyar, Am. Miner. 77 (1992) 1087.
[38] E. Jarosewich, J.A. Nelen, J.A. Norberg, Geostandard. Newslett. 4 (1980) 43.